Available online at www.sciencedirect.com
ScienceDirect
Journal of Solid State Chemistry 180 (2007) 1011–1019
JOURNAL OF SOLID STATE CHEMISTRY
www.elsevier.com/locate/jssc

Synthesis and structural study of a new NASICON-type solid solution: $Li_{1-x}La_{x/3}Zr_2(PO_4)_3$

M. Barré[a], M.P. Crosnier-Lopez[a,*], F. Le Berre[a], E. Suard[b], J.L. Fourquet[a]

[a]*Laboratoire des Oxydes et Fluorures (UMR CNRS 6010), Institut de Recherche en Ingénierie Moléculaire et Matériaux Fonctionnels (FR CNRS 2575), Faculté des Sciences et Techniques, Université du Maine, Av. O. Messiaen, 72085 Le Mans Cedex 9, France*
[b]*Institut Lauë-Langevin, 6 rue G. Horowitz, 38042 Grenoble Cedex 9, France*

Received 6 November 2006; received in revised form 21 December 2006; accepted 24 December 2006
Available online 9 January 2007

Abstract

A new complete solid solution of NASICON-type compounds between $LiZr_2(PO_4)_3$ and $La_{1/3}Zr_2(PO_4)_3$ was evidenced with the general formula $Li_{1-x}La_{x/3}Zr_2(PO_4)_3$ ($0 \leqslant x \leqslant 1$). These phases were synthesized by a complex polymerizable method and structurally characterized from Rietveld treatment of their X-ray and neutron powder diffraction data. This solid solution results from the substitution mechanism $Li^+ \rightarrow 1/3La^{3+} + 2/3\square$ leading to an increase of the vacancies number correlated to an increase of the La content. According to this substitution mechanism, the general formula can then be written $Li_{1-x}La_{x/3}\square_{2x/3}Zr_2(PO_4)_3$ ($0 \leqslant x \leqslant 1$) in order to underline the correlation between the La content and the vacancies rate. For all the compounds, the structure is clearly related to that of the NASICON family with three crystallographic domains evidenced. For $0 \leqslant x \leqslant 0.5$, all the members adopt at high temperature the typical NASICON-type structure (s.g. $R\bar{3}c$), while at lower temperature, their structure distorts to a triclinic form (s.g. C $\bar{1}$), as observed for $LiZr_2(PO_4)_3$ prepared above 1100 °C. Moreover, in this domain, the reversible transition is clearly soft and the transition temperature strongly depends of the x value. For $0.6 \leqslant x \leqslant 0.9$, the compounds crystallize in a rhombohedral cell (s.g. $R\bar{3}$), while for $x = 1$, the phase $La_{1/3}Zr_2(PO_4)_3$ is obtained (s.g. $P\bar{3}$, $Z = 6$, $a = 8.7378(2)$ Å, $c = 23.2156(7)$ Å).

This paper is devoted to the structure analysis of the series $Li_{1-x}La_{x/3}Zr_2(PO_4)_3$ ($0 \leqslant x \leqslant 1$), from X-ray and neutron powder thermo diffraction and transmission electron microscopy (TEM) studies.

Keywords: NASICON-type structure; $LiZr_2(PO_4)_3$; $La_{1/3}Zr_2(PO_4)_3$; Thermal X-ray and neutron powder diffraction; Transmission electron microscopy

1. Introduction

The crystal structure of NASICON-type phases, of general formula $A_xM_2(XO_4)_3$, can be described from corner-sharing of MO_6 octahedra and XO_4 tetrahedra (Fig. 1). The three-dimensional framework $M_2(XO_4)_3$ obtained delimits large cavities which can be occupied by various A cations. Two main types of cavities, $M1$ and $M2$, are often considered: the $M1$ cavity, one per formula unit, is located between two MO_6 octahedra along the c-axis forming ribbons $O_3MO_3AO_3MO_3$, while the $M2$ cavity, three per formula unit, is situated between these ribbons. In this NASICON family, the $RE_{1/3}Zr_2(PO_4)_3$ compounds, first pointed out by Alami Talbi et al. [1] in 1994, were found recently to be RE^{3+} ionic conductors [2]: since RE^{3+} ions occupy only 1/3 of the Li sites in $LiZr_2(PO_4)_3$, the RE^{3+} migration could then be expected due to the great number of available vacancies. One of these compounds, the $La_{1/3}Zr_2(PO_4)_3$ phase, holds a particular place: indeed, our research group shows in a recent paper that it is the only one to crystallize at room temperature in the $P\bar{3}$ space group [3], a new one in the NASICON family. Moreover, by increasing the temperature, $La_{1/3}Zr_2(PO_4)_3$ presents a structural transition [4a] from $P\bar{3}$ to $P\bar{3}c1$ space groups, transition induced by the La^{3+} ion ability to move in the $[Zr_2(PO_4)_3]^-$ network despite its ionic size. Taking into account this phenomenon, we chose to study the new series $Li_{1-x}La_{x/3}Zr_2(PO_4)_3$ ($0 \leqslant x \leqslant 1$) by hoping that the

*Corresponding author. Fax: +33 2 43 83 35 06.
E-mail address: marie-pierre.crosnier-lopez@univ-lemans.fr (M.P. Crosnier-Lopez).

0022-4596/$ - see front matter © 2007 Elsevier Inc. All rights reserved.
doi:10.1016/j.jssc.2006.12.032

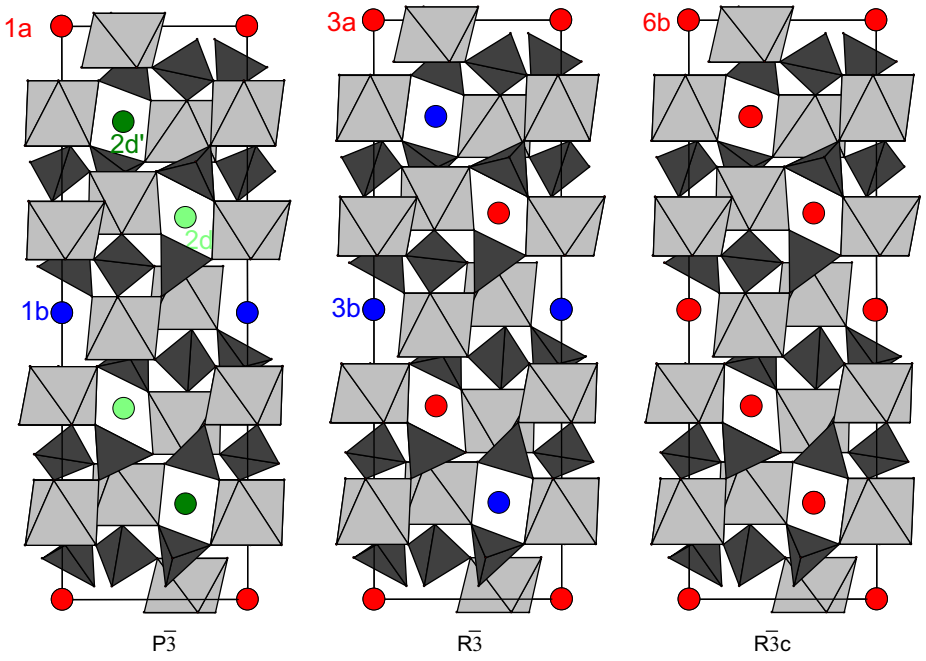

Fig. 1. Projection of the NASICON-type structure in the three space groups $P\bar{3}$, $R\bar{3}$ and $R\bar{3}c$ showing the different $M1$ sites available for the A cations in a preserved $[Zr_2(PO_4)_3]^-$ framework.

available vacancies created by the substitution mechanism between Li^+ and La^{3+} would support the migration of the conducting species. This paper is devoted to the structural properties with results based on Rietveld treatment of the X-ray and neutron diffraction powder patterns and transmission electron microscopy study while the ionic conductivity and the ^{31}P NMR measurements will be presented in a forthcoming paper.

2. Experimental

2.1. Sample preparation

Several members of the series $Li_{1-x}La_{x/3}Zr_2(PO_4)_3$ ($x = 0$–1.0 every 0.1) were synthesized in powder form from $^7Li_2CO_3$, dried La_2O_3 (1000 °C overnight), $ZrOCl_2 \cdot 8H2O$ and $NH_4H_2PO_4$ in stoichiometric ratios using a complex polymerizable method [5] as described in our previous paper [3]. ^7Li was used to reduce the absorption cross-section for neutron experiments. The molar ratios employed for citric acid (CA) and ethylene glycol (EG) were, respectively, $CA/M = 15/1$ ($M = [La]+[Zr]+[Li]$) and $CA/EG = 1/4$. The black precursor obtained after the gel calcination at 350 °C was ground and two successive annealings were performed in a furnace at 800 °C for 6 h, then at 1000 °C for the same time. The powder obtained was then pelletized and heated for 4 h at 1200 °C for $0.0 \leqslant x \leqslant 0.5$, and for higher x values, ($0.6 \leqslant x \leqslant 0.9$) at only 1100 °C for a longer time (6 h). One can notice that a better crystallization can be obtained by increasing temperature and time of annealing but that led always to the formation of some impurities, as ZrP_2O_7 and $Zr_2O(PO_4)_3$. The continuous evolution of the cell parameters between the first member $LiZr_2(PO_4)_3$ and the last member $La_{1/3}Zr_2(PO_4)_3$ as well as the purity of the samples revealed by the X-ray diffraction patterns allow us to retain the nominal value as the sample chemical composition.

2.2. Powder X-ray and neutron diffraction

The X-ray powder diffraction (XRD) patterns were recorded in air between room temperature and 1000 °C with Cu$K\alpha$ radiation on a PANalytical X'Pert Pro diffractometer equipped with the X'celerator detector and a high-temperature attachment Anton Paar HTK1200. Every 100 °C, the data were collected by step (0.017°) with a step time of 100 s scanning over an angular range of $7.0° < 2\theta < 100°$. The neutron diffraction patterns were recorded on ILL D2B high-resolution neutron diffractometer ($\lambda = 1.59601(1)$ Å, counting time 2 h, step scan 0.05° between 0.1° and 150.0° 2θ) in air at 700 °C for $Li_{0.7}La_{0.1}Zr_2(PO_4)_3$ ($x = 0.3$) and room temperature and 600 °C for $Li_{0.2}La_{0.8/3}Zr_2(PO_4)_3$ ($x = 0.8$).

Structure refinements were carried out by the Rietveld method from neutron data, using Fullprof [6] profile refinement software, with a pseudo-Voigt function applied to approximate the diffraction profiles and a manual background correction. The La content is fixed to its nominal value due to the small quantity and the low sensibility of the neutrons diffraction data concerning the Re content. We test structure refinements from XRD data but acceptable reliability factors can be obtained only with applying "soft constrained" Zr–O and P–O distances due to the precision of the light atom positional parameters

(O and P). However, better lanthanum localization is obtained from XRD data, so we tried to combine the two data files to approach the solution as well as possible. In addition, the evolutions of the parameters versus temperature and versus x at 800 °C are made only from XRD data, since we have more experimental points.

2.3. Transmission electron microscopy

Transmission electron microscopic (TEM) studies (selected area electron diffraction—SAED) were carried out on the phase $Li_{0.4}La_{0.2}Zr_2(PO_4)_3$ ($x = 0.6$) compound using a JEOL 2010 electron microscope operating at 200 kV and equipped with a side entry $\pm 30^\circ$ double tilt specimen holder. The sample was ultrasonically dispersed in butanol and a drop of the suspension was placed on a Cu grid with a holey carbon film. A complete study, recently published by our group on the phase $La_{1/3}Zr_2(PO_4)_3$ [4b] revealed a rapid transformation under the beam of the sample as soon as the crystallite is illuminated by the electron beam. This transformation implies the displacement of the two La^{3+} cations in a preserved classical $[Zr_2(PO_4)_3]^-$ network. The $Li_{0.4}La_{0.2}Zr_2(PO_4)_3$ compound is then investigated by TEM technique (SAED) in order to see if a similar transformation occurs, and no study was realized for the terms $x \leqslant 0.5$, because of their structural change with temperature (C $\bar{1} \rightarrow R\bar{3}c$), as described hereafter.

3. Results and discussion

3.1. For $0 \leqslant x \leqslant 0.5$

3.1.1. Powder X-ray and neutron diffraction

All the compounds present at room temperature a distortion of the classical rhombohedral NASICON-type, as $LiZr_2(PO_4)_3$ prepared at high temperature ($\geqslant 1100$ °C): above 60 °C, $LiZr_2(PO_4)_3$ adopts the typical NASICON structure (s.g. $R\bar{3}c$ — α variety) [7] while at lower temperature, its structure distorts to a triclinic form (s.g. C $\bar{1}$ — α' variety) [8] with the same linkage topology. At low temperature, the patterns of all the synthesized compounds present always a mixture of the two forms and their treatment with a "two phases" option is essential to index all the hkl lines. As an example, a zoom near $2\theta = 20^\circ$ of the XRD patterns of $Li_{0.7}La_{0.1}Zr_2(PO_4)_3$ ($x = 0.3$) between room temperature and 800 °C is shown on Fig. 2, revealing the overlapping of the lines belonging to the two varieties and the progressive disappearance of the C $\bar{1}$ form with increasing the temperature: at low temperature, the C $\bar{1}$ variety largely dominates, while as of 600 °C, the patterns can be fitted with only the rhombohedral variety. The coexistence of the two forms is observed in a very large temperature range (≈ 500 °C) meaning that the reversible triclinic-rhombohedral transition is soft (Table 1). Moreover, for all these compositions ($0 \leqslant x \leqslant 0.5$), the thermal domain of coexistence of the two

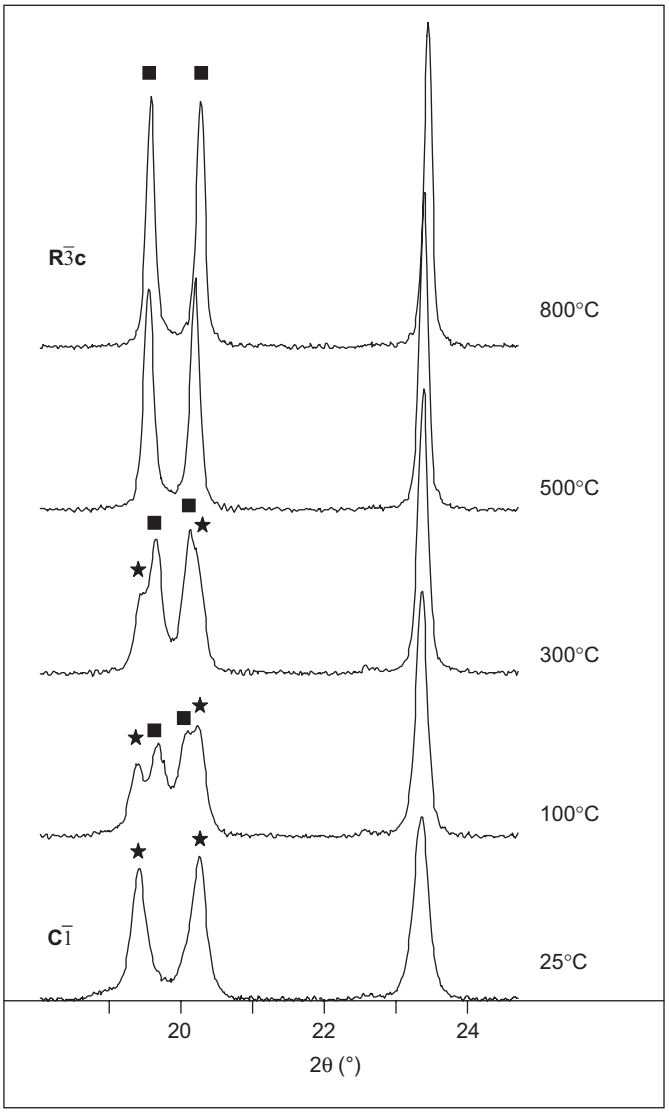

Fig. 2. XRD patterns for $Li_{0.7}La_{0.1}Zr_2(PO_4)_3$ ($x = 0.3$) at several temperatures showing the progressive disappearance of the C $\bar{1}$ variety in favor of the $R\bar{3}c$ variety when the temperature increases.

varieties C $\bar{1}$ and $R\bar{3}c$ is clearly dependent of the lanthanum content, as one can see on the Table 1.

At low temperature, Rietveld pattern refinements are difficult since an important overlapping of the lines is observed, nevertheless acceptable results can be obtained from XRD data with the pattern matching mode for the two varieties. As an example, the evolution versus temperature of the hexagonal cell parameters ($R\bar{3}c$ variety) followed on the whole temperature range is drawn on the Fig. 3 for the member $Li_{0.7}La_{0.1}Zr_2(PO_4)_3$ ($x = 0.3$) and reveal two very different regions either side of 600 °C. As encountered for $R\bar{3}c$ NASICON [9] phases, the a and c parameters have opposite variations in good agreement with the literature for NASICON-type phases, with a decrease of the a parameter and an increase of the c parameter, implying however a small volume expansion (from $V = 1515.7\,\text{Å}^3$ at 100 °C to $V = 1529.1\,\text{Å}^3$ at 1000 °C). Expansion coefficients α_p in the two regions can

Table 1
Thermal domain of coexistence for the two varieties triclinic-rhombohedral for $0.1 \leqslant x \leqslant 0.5$ (the vertical bar represents the temperature above which one single phase is observed)

T (°C) / x	100	200	300	400	500	600	700	800
0.1	C $\bar{1}$ + R $\bar{3}$ c				R $\bar{3}$ c			
0.2	C $\bar{1}$ + R $\bar{3}$ c				R $\bar{3}$ c			
0.3	C $\bar{1}$ + R $\bar{3}$ c				R $\bar{3}$ c			
0.4	C $\bar{1}$ + R $\bar{3}$ c					R $\bar{3}$ c		
0.5	C $\bar{1}$ + R $\bar{3}$ c							R $\bar{3}$ c

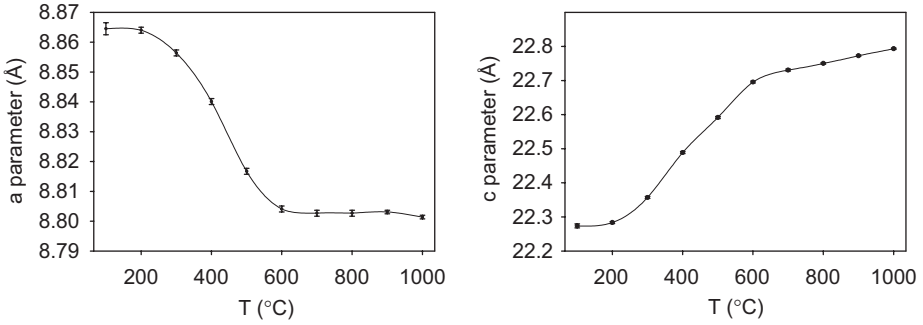

Fig. 3. Evolution versus temperature of the hexagonal cell parameters for the rhombohedral $R\bar{3}c$ variety of $Li_{0.7}La_{0.1}Zr_2(PO_4)_3$ ($x = 0.3$) from XRD data.

be calculated from the formula $\alpha p = (1/p)\,(dp/dT)$: between 100 and 600 °C, $\alpha_a = -13.63 \times 10^{-6}\,°C^{-1}$ and $\alpha_c = 37.87 \times 10^{-6}\,°C^{-1}$, and, between 600 °C and 1000 °C, $\alpha_a = -0.77 \times 10^{-6}\,°C^{-1}$ and $\alpha_c = 10.75 \times 10^{-6}\,°C^{-1}$. Indeed, many authors studied their thermal behavior [9,10], and more particularly the influence of the order/disorder of the *A* cations and the vacancies. However, even if the mechanism is still under investigations, they showed that thermal expansion of these phases is clearly anisotropic and depend in general of the space group: for the compounds crystallizing in the $R\bar{3}c$ space group, a contraction of the *a* axis and an expansion of the *c*-axis is observed, while for those crystallizing in the $R\bar{3}$ space group, an inverse situation is encountered. This seems to be due to the opposite expansivities of filled and vacant *M*1 sites. In addition, some authors claimed that it can be due to a displacement of *A* cations in the framework [11], while others think that the way of preparation can even influence the thermal behavior [9b].

At 700 °C, a complete $R\bar{3}c$ structure refinement for the member $Li_{0.7}La_{0.1}Zr_2(PO_4)_3$ ($x = 0.3$) is done from neutron data with the starting model [12] of the ideal NASICON atomic coordinates for the La^{3+} cations and the $[Zr_2(PO_4)_3]^-$ network. At this stage of the refinement, the reliability factors obtained are relatively high ($R_p = 14.0\%$ and $R_{Bragg} = 7.20\%$) and we do not succeed to localize the Li^+ cations despite the use of neutron diffraction data: Fourier difference maps show no residual negative peaks in spite of the lithium content (4.2 lithium atoms per unit cell). This situation is probably due to the fact that the two cations Li^+ and La^{3+} are located in the same cavities. Then, we choose to localize the lithium at a position proposed by Catti et al. [9a] in their thermal study of α-$LiZr_2(PO_4)_3$ and better reliability factors are obtained

Table 2
Structure refinements results for $Li_{0.7}La_{0.1}Zr_2(PO_4)_3$ ($x = 0.3$) at 700 °C from neutron diffraction data

	700 °C
Space group	$R\bar{3}c$ (no. 167)
Number of refined parameters	64
Peak shape, η	Pseudo-Voigt 0.64(2)
Cell parameters (Å)	$a = 8.7990(3)$
	$c = 22.7049(9)$
Half-width parameters	$u = 0.15(1)$
	$v = -0.33(1)$
	$w = 0.321(5)$
	$x = -0.001(1)$
Asymmetry parameters	$P_1 = 0.013(3)$
	$P_2 = 0.005(1)$
R_{Bragg} (%)	5.73
R_p (%)	12.9
R_{wp} (%)	11.6
R_{exp} (%)	5.14
χ^2	5.11

Table 3
$Li_{0.7}La_{0.1}Zr_2(PO_4)_3$ ($x = 0.3$): atomic coordinates in $R\bar{3}c$ (no. 167) at 700 °C from neutron diffraction data

	700 °C					
	Site	s.o.f.	x	y	z	B (10^{-2} Å^2)
Zr	12*c*	1	0	0	0.1439(1)	2.26(7)
P	18*e*	1	0.2864(4)	0	0.25	2.53(8)
O1	36*f*	1	0.1788(4)	−0.0241(4)	0.1963(1)	4.77(8)
O2	36*f*	1	0.1975(3)	0.1732(3)	0.0891(1)	3.99(8)
La	6*b*	0.100	0	0	0	9.3(9)
Li	36*f*	0.117	0.034(7)	0.152(6)	0.008(2)	1.0(8)

Bond valence calculations [13]: Zr:4.2, P: 5.4, O1: 2.1, O2: 2.0, La: 1.9, Li: 0.23.

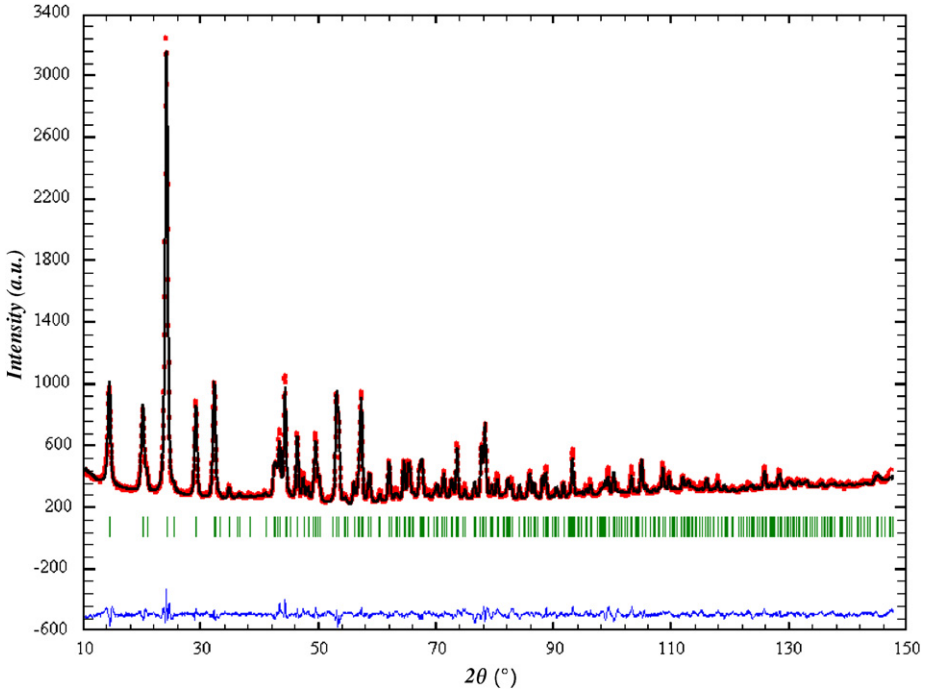

Fig. 4. Observed and calculated neutron patterns for $Li_{0.7}La_{0.1}Zr_2(PO_4)_3$ ($x = 0.3$) at 700 °C in the $R\bar{3}c$ space group. The difference pattern is shown below at the same scale and the vertical bars are related to the calculated Bragg reflection positions.

($R_p = 12.9$ and $R_{Bragg} = 5.73$) with refining the Li atomic coordinates. This Li position is all around the 3*b* lanthanum site (at 1.23 Å) and its environment is constituted by only two close oxygen atoms (2.24 and 2.29 Å), the two others being further (2.44 and 2.54 Å). Final structure refinement results are gathered in Table 2 while atomic coordinates are given in Table 3 and the corresponding experimental, calculated and difference profiles are shown in Fig. 4. In this structure, classical interatomic distances and valence sums [13] are obtained for Zr, P and O (respectively, 4.2, 5.4, 2.1 and 2.0), but La cations partially filling the 6*b* site (10%) in a six-fold coordination present a too low valence sum (1.9) and a too large B_{iso} value (9.3(9)) for such heavy cations. This situation, already encountered for many A cations in $A_xM_2(XO_4)_3$ NASICON-type phases [7,9b,10e,14], can be correlated to the size of the antiprism O_6 which would be able to accommodate larger *A* cations.

3.2. For $0.6 \leqslant x \leqslant 0.9$

3.2.1. Powder X-ray and neutron diffraction

All the diffraction patterns could be fitted on the basis of the expected rhombohedral cell ($a \approx 8.7$ and $c \approx 23.0$ Å), but the observed extinction conditions are inconsistent with the $R\bar{3}c$ space group usually used to describe a NASICON-type structure: for example, the presence of two diffraction lines (003) and (101) at low 2θ angle (at, respectively, 11.5° and 12.3° on the XRD pattern) (Fig. 5), prevents the *c*-axis glide plane. Then, we start the Rietveld calculations in the $R\bar{3}$ space group: the lowering of the symmetry ($R\bar{3}c$ to $R\bar{3}$) is due to an ordering of the cations and the vacancies on the two available sites, 3*a* and 3*b* (Fig. 1) of the $R\bar{3}$ space group, while in the typical NASICON $R\bar{3}c$ space group, the A cations and the vacancies are located on the same site (6*b*). The calculations are made for two temperatures (room temperature and 600 °C) for the member

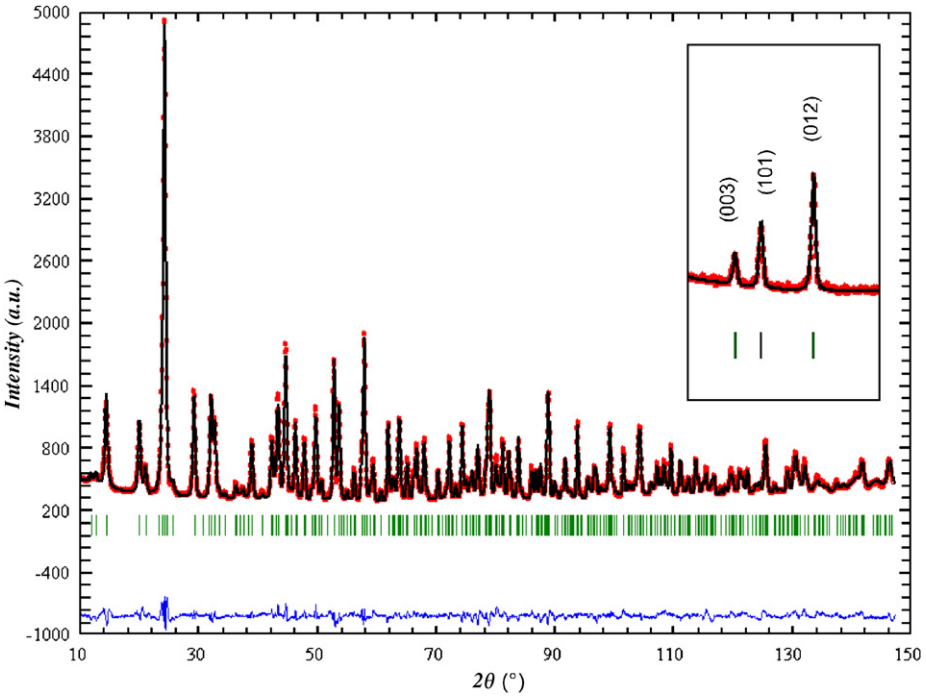

Fig. 5. Observed and calculated neutron diffraction pattern for $Li_{0.2}La_{0.8/3}Zr_2(PO_4)_3$ ($x = 0.8$) in the $R\bar{3}$ space group at room temperature, with the difference pattern shown below at the same scale (vertical bars are related to the calculated Bragg reflection positions). The inserted zoom presents two diffraction lines (003) and (101) of the XRD pattern at low 2θ angle inconsistent with the typical $R\bar{3}c$ NASICON space group. As one can see, these lines are much more intense on the XRD pattern than on the neutron diffraction pattern.

Table 4
Structure refinements results for $Li_{0.2}La_{0.8/3}Zr_2(PO_4)_3$ ($x = 0.8$) at room temperature and 600 °C from neutron diffraction data

	Room temperature	600 °C
Space group	$R\bar{3}$(no. 148)	
Number of refined parameters	60	66
Peak shape, η	Pseudo-Voigt 0.41(2)	Pseudo-Voigt 0.49(2)
Cell parameters (Å)	$a = 8.7161(1)$ $c = 23.0729(5)$	$a = 8.7365(2)$ $c = 23.0754(6)$
Half-width parameters	$u = 0.125(4)$ $v = -0.29(1)$ $w = 0.302(4)$ $x = -0.003(1)$	$u = 0.141(5)$ $V = -0.36(1)$ $w = 0.324(4)$ $x = -0.002(1)$
Asymmetry parameters	$P_1 = 0.010(3)$ $P_2 = 0.004(1)$	$P_1 = 0.005(3)$ $P_2 = 0.004(1)$
R_{Bragg} (%)	5.15	4.69
R_p (%)	9.22	9.91
R_{wp} (%)	9.57	9.87
R_{exp} (%)	3.16	3.69
χ^2	9.20	7.14

$Li_{0.2}La_{0.8/3}Zr_2(PO_4)_3$ ($x = 0.8$) with the atomic positions for all the ions taken from the model of $Ca_{0.5}Ti_2(PO_4)_3$ [15]. At the beginning of the refinements, the La^{3+} content is equally distributed on the two sites 3*a* and 3*b* and is allowed to be refined with constraint to its nominal value. The calculation progressively empties the 3*a* site in favor of the 3*b* site. This situation differs from that of the compound $La_{1/3}Ti_2(PO_4)_3$ [16] where the two La^{3+} ions are only distributed on the 3*a* site. For both temperatures, the reliability factors converge to reasonable values listed in Table 4, although we did not succeed in locating the Li^+ cations in the cell. Final atomic coordinates, sof, B_{iso} values and bond valence calculation [13] results are gathered in Table 5. A good minimization of the difference between the experimental and the calculated neutron patterns is observed, as shown on Fig. 5 for room temperature. The two octahedra ZrO_6 are regular with Zr–O distances ranging from 2.02(1) and 2.11(1) Å for Zr1 and 2.02(1) and 2.13(1) Å for Zr2, while the P–O distances are ranging from 1.49(1) to 1.53(1) Å leading to good bond valence values for these cations as for the anions at room temperature (Table 5). At 600 °C, the calculated distances are very similar, respectively, 2.01(1)–2.13(1) and 2.01(1)–2.14(1) Å for the two octahedra $Zr1O_6$ and $Zr2O_6$, and 1.48(1)–1.54(1) Å for the tetrahedral PO_4. Due to the large size of the antiprism $O4_6$ where the lanthanum cations are located, a large B_{iso} value is obtained for La^{3+} (5.9(5) at room temperature and 6.3(7) at 600 °C) correlated with a small bond valence value (2.2 at room temperature and 2.0 at 600 °C) which was already observed in similar phases [7,9b,10e,14]. It must be noted that, for other *x* values of this domain composition, the localization of the lanthanum ions is not affected by the lithium content since the 3*a* site is always empty whatever the composition. Moreover, thermal diffraction measurements show no modification of the lanthanum distribution, since the 3*a* site remains empty, meaning that no structural transition, as observed for $La_{1/3}Zr_2(PO_4)_3$, is evidenced. Finally, the evolution of the cell parameters from XRD

Table 5
$Li_{0.2}La_{0.8/3}Zr_2(PO_4)_3$ ($x = 0.8$): atomic coordinates in $R\bar{3}$ space group at room temperature and 600 °C from neutron diffraction data

	Room temperature						600 °C					
	Site	s.o.f.	x	y	z	B (10^{-2} Å^2)	Site	s.o.f	x	y	z	B (10^{-2} Å^2)
Zr1	6*c*	1	0	0	0.1425(2)	0.58(7)	6*c*	1	0	0	0.1413(2)	0.72(6)
Zr2	6*c*	1	0	0	0.6485(2)	0.67(8)	6*c*	1	0	0	0.6494(2)	0.72(6)
P	18*f*	1	0.2829(4)	−0.0067(5)	0.2484(2)	0.78(5)	18*f*	1	0.2853(5)	−0.0036(7)	0.2488(3)	1.08(6)
O1	18*f*	1	0.1586(5)	0.9392(5)	0.1963(2)	2.42(9)	18*f*	1	0.1646(8)	0.9452(7)	0.1954(2)	3.6(1)
O2	18*f*	1	0.0049(5)	0.8108(5)	0.6979(1)	2.00(7)	18*f*	1	0.0096(6)	0.8157(7)	0.6989(2)	2.7(1)
O3	18*f*	1	0.2196(4)	0.1608(4)	0.0960(1)	0.79(6)	18*f*	1	0.2161(6)	0.1649(6)	0.0956(2)	1.7(1)
O4	18*f*	1	0.8152(4)	0.8183(4)	0.5875(1)	0.80(6)	18*f*	1	0.8196(6)	0.8158(6)	0.5875(2)	1.5(1)
La	3*b*	0.533	0	0	0.5	5.9(5)	3*b*	0.533	0	0	0.5	6.3(7)

Bond valence calculations [13]: room temperature : Zr_1:4.1, Zr_2:4.1, P: 5.2, O1: 1.9, O2: 2.2, O3: 2.1, O4: 2.0, La: 2.2; 600 °C: Zr1:4.2, Zr2:4.1, P: 5.3, O1: 1.8, O2: 2.2, O3: 2.2, O4: 2.0, La: 2.0.

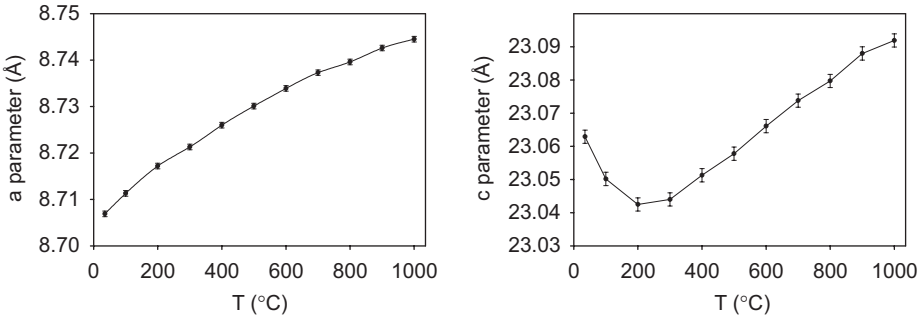

Fig. 6. Evolution of the cell parameters for $Li_{0.2}La_{0.8/3}Zr_2(PO_4)_3$ ($x = 0.8$) in the $R\bar{3}$ space group from XRD data.

data for this compound is plotted on the Fig. 6 and the mean thermal expansion coefficients are low and both positive between room temperature and 1000 °C: $\alpha_a = 4.48 \times 10^{-6}$ and $\alpha_c = 1.30 \times 10^{-6}\,°C^{-1}$. If below 200 °C a classical anisotropic thermal behavior of an $R\bar{3}$ NASICON phase is observed, above 200 °C, an expansion of the c parameter occurs. Taking into account these two different regions observed either side of 200 °C, two α_c thermal expansion coefficients can be calculated: between 35 and 200 °C, $\alpha_c = -5.36 \times 10^{-6}\,°C^{-1}$, while between 200 and 1000 °C, $\alpha_c = 2.68 \times 10^{-6}\,°C^{-1}$. The temperature corresponding to the minimal c value (about 200 °C for the phase $Li_{0.2}La_{0.8/3}Zr_2(PO_4)_3$ $-x = 0.8$) increases with the lithium content (for example, for $x = 0.6$ this minimum is close to 450 °C). On another hand, if we compare the O–O height along c-axis of the oxide antiprism O_6 surrounding the $M1$ position for the two sites 3*a* (O3–O3) and 3*b* (O4–O4) for the phase $Li_{0.2}La_{0.8/3}Zr_2(PO_4)_3$, we see that between the room temperature and 600 °C, the two sites height is preserved in spite of their different occupancy rate (O3–O3 height: at RT, 4.41 Å and at 600 °C, 4.43 Å; O4–O4 height: at RT, 4.04 Å and at 600 °C, 4.04 Å), in good agreement with the low thermal coefficient α_c.

3.2.2. Transmission electron microscopy

The reconstitution of the reciprocal space of various crystallites of $Li_{0.4}La_{0.2}Zr_2(PO_4)_3$ ($x = 0.6$) leads always to an hexagonal cell with the following parameters $a \approx 8.7$ and $c \approx 23.0$ Å. The systematic absences are characteristic of a rhombohedral extinction symbol R- - -, compatible with the centrosymetric space groups $R\bar{3}$ (no. 148) and $R\bar{3}m$ (no. 166) and the corresponding acentric ones. As discussed in the X-ray paragraph, the condition on the $0\,0\,l$ spots, $l = 6\,n$, implying the existence of c-axis glide is clearly not respected, preventing the $R\bar{3}c$ space group. Typically, SAED patterns of two different zone axis orientations are shown in Fig. 7. No transformation like that observed for $La_{1/3}Zr_2(PO_4)_3$ [4b] under the beam was observed for this sample.

3.3. For $x = 1$

The phase $La_{1/3}Zr_2(PO_4)_3$ [3] is obtained (s.g. $P\bar{3}$, $Z = 6$, $a = 8.7378(2)$ Å, $c = 23.2156(7)$ Å). In this structure, the two La^{3+} are found quasiordered along the c-axis at room temperature in the $M1$ cavities: 1 La^{3+} in the La1 site (1*a*), 0.56(1) in the La2 site (1*b*) and the remaining 0.44(1) in the La3 one (2*d*) (Fig. 1). By increasing the temperature, the La3 site progressively empties in favor of the La2 site [4a], leading at 1000 °C to a structural transition from $P\bar{3}$ to $P\bar{3}c1$, with the two La^{3+} ions located along the c-axis (2*b* site). Between room temperature and 1000 °C, the thermal expansion coefficients α_a and α_c of $La_{1/3}Zr_2(PO_4)_3$ are both positive and very small (close to $2 \times 10^{-6}\,°C^{-1}$) compared

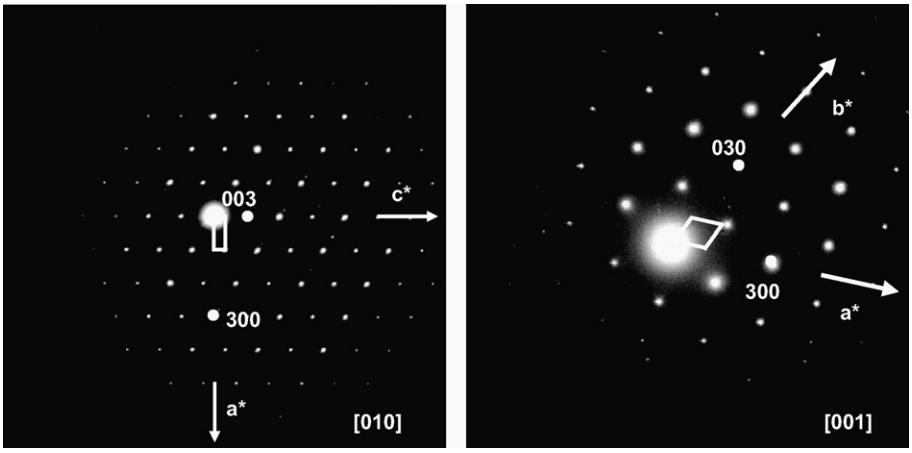

Fig. 7. Typical SAED patterns of $Li_{0.4}La_{0.2}Zr_2(PO_4)_3$ ($x = 0.6$) with two different [010] and [001] zone axis.

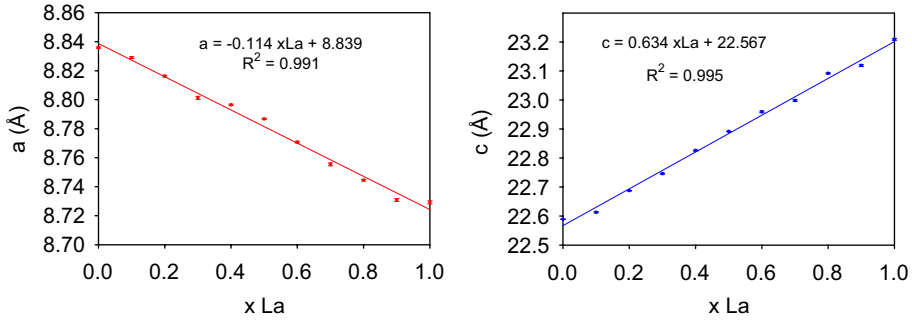

Fig. 8. Evolution of hexagonal cell parameters versus composition at 800 °C from XRD data.

to those of α-$LiZr_2(PO_4)_3$ ($\alpha_a \approx -4.54 \times 10^{-6}$ and $\alpha_c \approx 27.7 \times 10^{-6}\,°C^{-1}$ at 400 °C) [9a].

3.4. For $0 \leqslant x \leqslant 1$

Finally, despite the existence of these different crystallographic domains, it is possible to plot at 800 °C the evolution of cell parameters a and c versus composition from XRD data (Fig. 8), since at this temperature, all the compounds crystallize in an hexagonal cell: space group $R\bar{3}c$ for $0 \leqslant x \leqslant 0.5$, space group $R\bar{3}$ for $0.6 \leqslant x \leqslant 0.9$ and space group $P\bar{3}$ for $x = 1$. Despite the different space groups used in the three domains, both evolutions are linear: the a parameter decreases while the c parameter increases. These two opposite behaviors can be explained by considering electrostatic repulsion and occupation number of the cationic A site as explained by Delmas [17]. Indeed, the substitution mechanism $Li^+ \rightarrow 1/3La^{3+} + 2/3\square$ leads to an increase of both vacancies number and La content. This variation of the vacancies number with x can be correlated with a decrease of the cation–cation repulsion between the ribbons implying a shortening of the a parameter. Concerning the expansion of the c parameter, it is influenced by two additional simultaneous effects: the occupation number of the A cationic site which decreases with the lanthanum content and the substitution of small Li^+ cations by a larger one La^{3+} (respectively, 0.76 and 1.032 Å for a six coordination number [18]). This leads both to an increase of the c parameter.

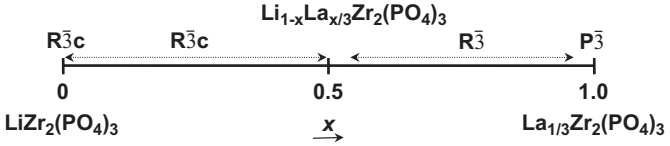

Fig. 9. Schematic drawing of the space group evolution at 800 °C in the solid solution $Li_{1-x}La_{x/3}Zr_2(PO_4)_3$ ($0 \leqslant x \leqslant 1$).

Taking into account these evolutions, we can conclude that the solid solution between $LiZr_2(PO_4)_3$ and $La_{1/3}Zr_2(PO_4)_3$ is continuous (Fig. 9).

4. Conclusion

A new complete NASICON solid solution $Li_{1-x}La_{x/3}Zr_2(PO_4)_3$ ($0 \leqslant x \leqslant 1$) is evidenced and results from the substitution mechanism $Li^+ \rightarrow 1/3La^{3+} + 2/3\square$ between $LiZr_2(PO_4)_3$ and $La_{1/3}Zr_2(PO_4)_3$. The compounds were synthesized by a complex polymerizable method and structurally characterized from Rietveld treatment of their X-ray and neutron powder diffraction data. Their structure is clearly related to that of the NASICON family but three

crystallographic domains can be evidenced. For $0 \leqslant x \leqslant 0.5$, the compounds adopt a similar behavior with that of $LiZr_2(PO_4)_3$ prepared above 1100 °C. At high temperature, the typical NASICON structure (s.g. $R\bar{3}c$ — α variety) is observed, while at lower temperature, the structure distorts to a triclinic form (s.g. C $\bar{1}$ — α' variety). This soft transition C $\bar{1} \rightarrow R\bar{3}c$ is reversible and dependent of the x value. For $0.6 \leqslant x \leqslant 0.9$, the compounds crystallize in a rhombohedral cell (s.g. $R\bar{3}$), the lowering of the symmetry being due to an ordering of the A cations and the vacancies. For $x = 1$, the phase $La_{1/3}Zr_2(PO_4)_3$ is obtained (s.g. $P\bar{3}$). This structural study is a new example of the flexibility of the NASICON framework and confirms the particular behavior of $La_{1/3}Zr_2(PO_4)_3$: a small Li insertion in $La_{1/3}Zr_2(PO_4)_3$ implies immediately an ordering of the lanthanum. On another hand, no transformation under the beam during the TEM study, as encountered for the lanthanum compound, can be evidenced. Ionic conductivity and ^{31}P NMR measurements are now in progress and will be presented in a forthcoming paper.

References

[1] M. Alami Talbi, R. Brochu, C. Parent, L. Rabardel, G. Le Flem, J. Solid State Chem. 110 (1994) 350.

[2] (a) S. Tamura, N. Imanaka, G. Adachi, J. Alloys Compds 323–324 (2001) 540;
(b) S. Tamura, N. Imanaka, G. Adachi, Solid State Ionics 154–155 (2002) 767.

[3] M. Barré, M.P. Crosnier-Lopez, F. Le Berre, J. Emery, E. Suard, J.L. Fourquet, Chem. Mater. 17 (2005) 6605.

[4] (a) M. Barré, F. Le Berre, M.P. Crosnier-Lopez, O. Bohnké, J. Emery, J.L. Fourquet, Chem. Mater. 18 (2006) 5486;
(b) M.P. Crosnier-Lopez, M. Barré, F. Le Berre, J.L. Fourquet, J. Solid State Chem. 179 (2006) 2714.

[5] (a) M.P. Pechini, US Patent 3330697, 1967.;
(b) M. Kakihana, J. Sol–Gel Sci. Technol. 6 (1996) 7.

[6] J. Rodriguez-Carvajal, Program FULLPROF.2K, Version 3.20, Institut Laüe- Langevin, Grenoble, 2005.

[7] M. Catti, S. Stramare, Solid State Ionics 136–137 (2000) 489.

[8] (a) J.E. Iglesias, C. Pecharroman, Solid State Ionics 112 (1998) 309;
(b) M. Catti, S. Stramare, R. Ibberson, Solid State Ionics 123 (1999) 173.

[9] (a) M. Catti, A. Comotti, S. Di Blas, Chem. Mater. 15 (2003) 1628;
(b) D.A. Woodcock, P. Lightfoot, R.I. Smith, J. Mater. Chem. 9 (1999) 2631.

[10] (a) S. Senbhagaraman, A.M. Umarji, J. Solid State Chem. 85 (1990) 169;
(b) D.A. Woodcock, P. Lightfoot, C. Ritter, Chem. Commun. (1998) 107;
(c) J. Alamo, J.L. Rodrigo, Solid State Ionics 63–65 (1993) 678;
(d) G.E. Lenain, H.A. McKinstry, J. Alamo, D.K. Agrawal, J. Mater. Sci. 22 (1987) 17;
(e) R. Brochu, M. El-Yacoubi, M. Louër, A. Serghini, M. Alami, D. Louër, Mater. Res. Bull. 32 (1) (1997) 15.

[11] K.V.G. Kutty, R. Asuvathraman, R. Sridharan, J. Mater. Sci. 33 (1998) 4007.

[12] D. Petit, P.H. Colomban, G. Collin, J.P. Boilot, Mater. Res. Bull 21-3 (1) (1986) 365.

[13] N.E. Brese, M. O'Keeffe, Acta Crystallogr. B 47 (1991) 192.

[14] (a) D.M. Bykov, E.R. Gobechiya, Yu.K. Kabalov, A.I. Orlova, S.V. Tomilin, J. Solid State Chem. 179 (2006) 3101;
(b) A. Aatiq, M. Ménétrier, L. Croguennec, E. Suard, C. Delmas, J. Mater. Chem. 12 (2002) 2971.

[15] S. Senbhagaraman, T.N. Guru Row, A.M. Umarji, J. Mater. Chem. 3 (3) (1993) 309.

[16] P. Lightfoot, D.A. Woodcock, J.D. Jorgensen, S. Short, Int. J. Inorg. Mater. 1 (1999) 53.

[17] (a) C. Delmas, R. Olazcuaga, G. Le Flem, P. Hagenmuller, Mater. Res. Bull. 16 (1985) 16;
(b) C. Delmas, J.C. Vala, R. Olazcuaga, G. Le Flem, P. Hagenmuller, Mater. Res. Bull. 16 (1981) 83.

[18] R.D. Shannon, Acta Crystallogr. Sect. A 32 (1976) 751.